Molecular, kinetic and thermodynamic characterization of Mycobacterium tuberculosis orotate phosphoribosyltransferase

ARTICLE *in* MOLECULAR BIOSYSTEMS · NOVEMBER 2011

Impact Factor: 3.21 · DOI: 10.1039/c1mb05402c · Source: PubMed

5 AUTHORS, INCLUDING:

Ardala Breda
Texas A&M University
17 PUBLICATIONS **116** CITATIONS
SEE PROFILE

Leonardo Rosado
Vrije Universiteit Brussel
16 PUBLICATIONS **68** CITATIONS
SEE PROFILE

Diógenes S dos Santos
Pontifícia Universidade Católica do Rio Gra…
198 PUBLICATIONS **3,125** CITATIONS
SEE PROFILE

Molecular BioSystems

Dynamic Article Links

Cite this: *Mol. BioSyst.*, 2012, **8**, 572–586

www.rsc.org/molecularbiosystems

PAPER

Molecular, kinetic and thermodynamic characterization of *Mycobacterium tuberculosis* orotate phosphoribosyltransferase†‡

Ardala Breda,[abc] Leonardo Astolfi Rosado,[abd] Daniel Macedo Lorenzini,[ab] Luiz Augusto Basso*[abc] and Diógenes Santiago Santos*[abc]

Received 27th September 2011, Accepted 18th October 2011
DOI: 10.1039/c1mb05402c

Tuberculosis (TB) is a chronic infectious disease caused mainly by *Mycobacterium tuberculosis*. The worldwide emergence of drug-resistant strains, the increasing number of infected patients among immune compromised populations, and the large number of latent infected individuals that are reservoir to the disease have underscored the urgent need of new strategies to treat TB. The nucleotide metabolism pathways provide promising molecular targets for the development of novel drugs against active TB and may, hopefully, also be effective against latent forms of the pathogen. The orotate phosphoribosyltransferase (OPRT) enzyme of the *de novo* pyrimidine synthesis pathway catalyzes the reversible phosphoribosyl transfer from 5′-phospho-α-D-ribose 1′-diphosphate (PRPP) to orotic acid (OA), forming pyrophosphate and orotidine 5′-monophosphate (OMP). Here we describe cloning and characterization of *pyrE*-encoded protein of *M. tuberculosis* H37Rv strain as a homodimeric functional OPRT enzyme. The *M. tuberculosis* OPRT true kinetic constants for forward reaction and product inhibition results suggest a Mono-Iso Ordered Bi–Bi kinetic mechanism, which has not been previously described for this enzyme family. Absence of detection of half reaction and isothermal titration calorimetry (ITC) data support the proposed mechanism. ITC data also provided thermodynamic signatures of non-covalent interactions between substrate/product and *M. tuberculosis* OPRT. These data provide a solid foundation on which to base target-based rational design of anti-TB agents and should inform us how to better design inhibitors of *M. tuberculosis* OPRT.

Introduction

Tuberculosis (TB) is a chronic infectious disease caused mainly by *Mycobacterium tuberculosis* (MTB),[1] killing over 2 million people annually,[2] with 8.9–9.9 million estimated cases in 2008, according to World Health Organization (WHO).[3] Patients' non-compliance to the current treatments, along with HIV infection emergence, leads to the occurrence of multi drug-resistant and extensively drug-resistant TB strains, and to an increasing number of new cases.[2] Recently, TB infections with totally resistant strains, denoted as TDR-TB have been described, which are resistant to all first and second line classes of anti-TB drugs tested.[4,5] Novel TB treatments should ideally be able to also eliminate latent forms of TB, estimated to affect 32% of world's population, that are a significant infection reservoir.[6]

Although being an ancient human disease,[7] little is known about the nutritional adaptability of MTB in the course of TB infection.[8,9] Whether MTB relies on complex nutrient molecules uptake from the host (salvage pathways) or on synthesis of essential molecules from simple and passive diffusible precursors (*de novo* synthesis pathways) is still not clear. In addition, the identity of inner and outer membrane transporters for essential nutrients in MTB is largely unknown, despite the availability of genetic data.[9] Nutrient starvation is considered an essential element for long-term survival of mycobacteria during latent infection,[10] in response to microenvironments such as necrotic or caseous regions of granuloma[9,11] that are remote from the cavity surface of host lungs, where the availability of oxygen and nutrients is likely to be restricted.[12]

[a] *Instituto Nacional de Ciência e Tecnologia em Tuberculose, Pontifícia Universidade Católica do Rio Grande do Sul, Porto Alegre, Rio Grande do Sul, Brazil*
[b] *Centro de Pesquisas em Biologia Molecular e Funcional, Pontifícia Universidade Católica do Rio Grande do Sul, Avenida Ipiranga 6900 Prédio 92A – TECNOPUC, 90619-900 Porto Alegre, Rio Grande do Sul, Brazil. E-mail: luiz.basso@pucrs.br, diogenes@pucrs.br; Fax: +55 51 3320 3629; Tel: +55 51 3320 3629*
[c] *Programa de Pós-Graduação em Biologia Celular e Molecular, Pontifícia Universidade Católica do Rio Grande do Sul, Porto Alegre, Rio Grande do Sul, Brazil*
[d] *Programa de Pós-Graduação em Medicina e Ciências da Saúde, Pontifícia Universidade Católica do Rio Grande do Sul, Porto Alegre, Rio Grande do Sul, Brazil*

† This work is dedicated to the memory of late Prof. Ir. Norberto Rauch, who is an example of an enterprising dean and a tireless champion of the advancement of teaching and science in Brazil.

‡ Electronic supplementary information (ESI) available. See DOI: 10.1039/c1mb05402c

The nucleotide metabolism is an essential pathway for microorganism viability; and the *de novo* pyrimidine biosynthesis has been shown to be required for cell invasion and virulence of obligatory parasites such as *Toxoplasma gondii*[13] and *Plasmodium vivax*,[14] in which disruption of this pathway leads to uracil auxotrophs that are completely avirulent.[13] Transcriptional profiling studies on MTB indicate the maintenance of DNA repair and replication processes that are expected to occur during latent TB replication rate[15–17] and reactivation.[18] However, free nucleotide uptake from the host may not be possible due to MTB intrinsic properties and due to pathology's characteristics[14] such as the tubercle structure in TB.[19]

Orotate phosphoribosyltransferase (OPRT, EC 2.4.2.10) catalyzes the fifth reaction in the *de novo* synthesis of pyrimidine nucleotides, in which orotate (OA) and 5′-phospho-α-D-ribose 1′-diphosphate (PRPP) are converted to orotidine 5′-monophosphate (OMP), and pyrophosphate (PP_i), in the presence of Mg^{2+} (Fig. 1). OPRT catalyzes the last step in this pathway for which there is no chemical intermediate that can be derived from the pyrimidine salvage pathway.[20] Accordingly, this reaction may be considered as a commitment step of the *de novo* pathway, which has been shown to be essential for survival of MTB and *Mycobacterium bovis* BCG.[21]

Here we describe cloning of *pyrE* (Rv0382c) from *M. tuberculosis*, and expression and purification of recombinant protein. Functional studies demonstrate that this gene encodes an OPRT (*Mt*OPRT) enzyme with homodimeric quaternary structure. Determination of true steady-state kinetic parameters for the forward reaction, product inhibition patterns, half-reaction measurements and isothermal titration calorimetry (ITC) measurements of substrate/product binding to *Mt*OPRT suggest that it follows a Mono-Iso Ordered Bi–Bi kinetic mechanism, which has not been previously described for any member of this enzyme family. ITC data also provided thermodynamic signatures of non-covalent interactions between substrate/product and *Mt*OPRT, which are consistent with catalytic loop motions upon substrate binding and product release that may represent the ISO mechanistic step. The results presented here should contribute to function-based design of *Mt*OPRT enzyme inhibitors. It is hoped that the results described here may contribute to a better understanding of the biology of MTB, and may also be useful to chemical biologists interested in designing loss-of-function (inhibitors) or gain-of-function (activators) chemical compounds to reveal the biological role of *Mt*OPRT in the context of whole MTB cells.

Results

*Mt*OPRT amplification, cloning, expression and purification

The nucleotide sequence of the insert was confirmed by automated sequencing, revealing a discrepancy between the *pyrE* gene sequence available at TubercuList (http://genolist.pasteur.fr/TubercuList/) database and our clone at position 99. The third base of the 33rd codon changed from thymine (TAT) given by the genome sequencing to cytosine (TAC) as described here. Nevertheless, both codons are for tyrosine, and it might have been introduced by PCR amplification or be a misannotation of the Rv0382c locus in MTB H37Rv.[22] SDS-PAGE analysis showed expression of *Mt*OPRT recombinant enzyme with an apparent subunit molecular mass of ~20 kDa in agreement with predicted molecular mass (18.8 kDa). *Mt*OPRT was purified to homogeneity by a three-step protocol (Table 1). *Mt*OPRT was desorbed from HiPrep Q-XL 16/10 anion exchange resin at 300 mM salt concentration. Eluted samples were concentrated and loaded on HiPrep 26/60 Sephacryl S-200 HR to remove salt from recombinant protein samples, which, however, was accompanied by significant activity loss (Table 1). Pooled fractions containing *Mt*OPRT were loaded on a HiLoad 16/10 Phenyl Sepharose HP hydrophobic interaction column, from which homogeneous recombinant protein eluted at 26–42% gradient of buffer A (660 mM salt concentration), yielding 6.65 mg (Table 1). Activity loss observed after the size exclusion chromatography step was reversed after hydrophobic interaction chromatography. Dialysis against buffer A prior to enzyme storage did not affect its specific activity.

Identification of *Mt*OPRT by mass spectrometry and molecular mass determination

Purified *Mt*OPRT digested with trypsin was submitted to LC-MS/MS analysis, and 343 spectra were identified for 8 peptides

Table 1 Purification of *Mt*OPRT from *E. coli* BL21(DE3). Typical purification protocol for 12 g wet cell paste from 3 L culture

Step	Total protein/ mg	Specific activity[a]/ U mg^{-1}	Total enzyme activity/ U	Yield/ %	Purification fold
Crude extract	131	8	1088.6	100	1
HP 16/10 Q XL	46.4	51	2354.4	216	6.4
Sephacryl S-200	10.6	40	423	39	5
Phenyl Sepharose HP	6.6	105	693	64	13

[a] One enzyme unit is the amount of *Mt*OPRT that converts 1 μmol of OA to OMP per minute at 25 °C.

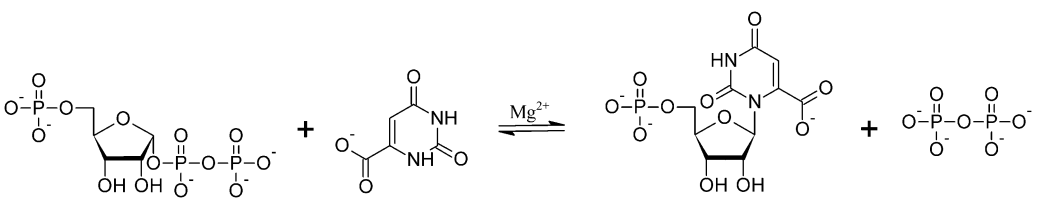

Fig. 1 OPRT catalyzed conversion of OA and PRPP into OMP and PP_i by the formation of an *N*-glycosidic bond in the presence of Mg^{2+}, the fifth step of pyrimidine *de novo* synthesis pathway.

from the *Mt*OPRT amino acid sequence (data not shown), representing 73% of the whole *Mt*OPRT sequence. Mass spectrometry spectra showed peaks corresponding to charged states (from 15^+ to 25^+) of *Mt*OPRT recombinant protein, and deconvolution of these spectra gave a single peak corresponding to an average molecular mass value of 18.761 Da for *Mt*OPRT (data not shown).

Analytical HPLC gel filtration

Recombinant active *Mt*OPRT was loaded on a Superdex 200 HR 10/30 size exclusion column using three distinct concentrations (7 μM, 11 μM and 53 μM), showing molecular masses of 38.67 kDa, 37.499 kDa and 36.01 kDa, according to data fitting to eqn (1) and (2). Molecular mass values divided by *Mt*OPRT subunit molecular mass (18.761 kDa) indicate that *Mt*OPRT has a homodimeric quaternary structure in solution, in the protein concentration range here presented.

Kinetic properties of recombinant *Mt*OPRT

Prior to embarking on determination of steady-state kinetic parameters for the forward reaction, the optimal concentration range of $MgCl_2$ to be employed in initial rate measurements was determined to be 15–30 mM (data not shown). Accordingly, $MgCl_2$ concentration was fixed at 20 mM for all further experiments. The true macroscopic steady-state kinetic constants for the forward reaction of *Mt*OPRT are summarized in Table 2. The apparent kinetic constants for the reverse reaction are also given in Table 2. The true kinetic parameters for forward reaction were determined from primary double-reciprocal plots of the steady-state initial velocity kinetics. The data were initially fitted to eqn (4) for a double-displacement (or Ping-Pong) bisubstrate kinetic mechanism, which is suggested by the apparently parallel lines pattern observed for both substrates (Fig. 2). $k_{catforward}/k_{catreverse}$ for *Mt*OPRT enzyme is 2.16 (Table 2), an indication that forward reaction is faster than the reverse one.

Half-reaction detection by PP_i consumption measurement

In case *Mt*OPRT followed a Ping-Pong mechanism in which the 5′-phosphate ribose moiety of PRPP would be transferred to *Mt*OPRT enzyme active site, detection of PP_i release in solution was assessed by a coupled assay. As a positive control, OA at saturating concentration (100 μM) was added to the reaction mixture, a condition in which PP_i release is certain to occur. As PRPP was varied (5–40 μM) in the presence of OA, an increase in 2-amino-6-mercapto-7-methylpurine formation was observed indicating that there was an increase in PP_i formation by *Mt*OPRT (Fig. 3). No significant activity could be detected when the experiment was performed under the same conditions in the absence of OA. These data show that there is no half-reaction in the absence of OA, thereby demonstrating that *Mt*OPRT cannot transfer 5′-phosphate ribose from PRPP to the enzyme active site in the absence of the second reaction substrate. Minimal activity detected is due to PRPP contamination with PP_i, largely accounted for by pre-incubation prior to adding *Mt*OPRT to start the reaction.

Enzymatic reaction mechanism determination by product inhibition assays

As there was ambiguity on the enzyme mechanism suggested by steady-state kinetics data in the absence of products and half-reaction measurements, product inhibition assays were carried out for the forward reaction, using both OMP and PP_i products as inhibitors (Table 3, and Fig. S1 and S2 of ESI‡).

Table 2 *Mt*OPRT and some homologues OPRTs kinetic parameters

		Ligand			
Organism	Kinetic constants	OA	PRPP	OMP	PP_i
Mycobacterium tuberculosis (Ping-Pong)	$K_M/\mu M$	10 ± 0.5	96 ± 4.1	2.6 ± 0.4[a]	16 ± 0.6[a]
	k_{cat}/s^{-1}	0.61 ± 0.01		0.280 ± 0.01[a]	0.280 ± 0.003[a]
	$k_{cat}/K_M/M^{-1}\ s^{-1}$	60 (±3) × 10^3	6.0 (±0.3) × 10^3	100 (±18.3) × 10^{3a}	10 (±0.7) × 10^{3a}
Mycobacterium tuberculosis (Ordered)	$K_M/\mu M$	9.4 ± 0.7	90 ± 6	—	—
	k_{cat}/s^{-1}	0.6 ± 0.02		—	—
	$k_{cat}/K_M/M^{-1}\ s^{-1}$	64 (±9) × 10^3	6.6 (±0.9) × 10^3	—	—
Plasmodium falciparum[14]	$K_M/\mu M$	18.2 ± 0.9	28.6 ± 1.3	25.1 ± 0.7	14.3 ± 0.1
	k_{cat}/s^{-1}	3.0 ± 0.1	3.2 ± 0.1	2.6 ± 0.1	1.3 ± 0.1
	$k_{cat}/K_M/M^{-1}\ s^{-1}$	16.4 × 10^6	11.3 × 10^6	10.2 × 10^6	9.4 × 10^6
Saccharomyces cerevisiae[23]	$K_M/\mu M$	18.7 ± 3.4	18.2 ± 4.5	3.4 ± 0.3	30.6 ± 2.5
	k_{cat}/s^{-1}	111 ± 5		35 ± 0.5	
	$k_{cat}/K_M/M^{-1}\ s^{-1}$	5.9 × 10^6	6.1 × 10^6	10 × 10^6	1.1 × 10^6
Salmonella typhimurium[24]	$K_M/\mu M$	27.5	44.1	3.1	31.1
	k_{cat}/s^{-1}	—	—	—	—
	$k_{cat}/K_M/M^{-1}\ s^{-1}$	—	—	—	—
Salmonella typhimurium[25]	$K_M/\mu M$	20 ± 2	18 ± 3	2.1 ± 0.2	47 ± 7
	k_{cat}/s^{-1}	—	—	—	—
	$k_{cat}/K_M/M^{-1}\ s^{-1}$	—	—	—	—
Corynebacterium ammoniagenes[26]	$K_M/\mu M$	33.09	63.53	44.84	36.1
	k_{cat}/s^{-1}	—	—	—	—
	$k_{cat}/K_M/M^{-1}\ s^{-1}$	—	—	—	—
Homo sapiens[27]	$K_M/\mu M$	2.1 ± 0.12	—	0.23 ± 0.87	—
	k_{cat}/s^{-1}	4.0	—	16	—
	$k_{cat}/K_M/M^{-1}\ s^{-1}$	—	—	—	—

[a] Values corresponding to apparent steady-state kinetic constants for the reverse reaction.

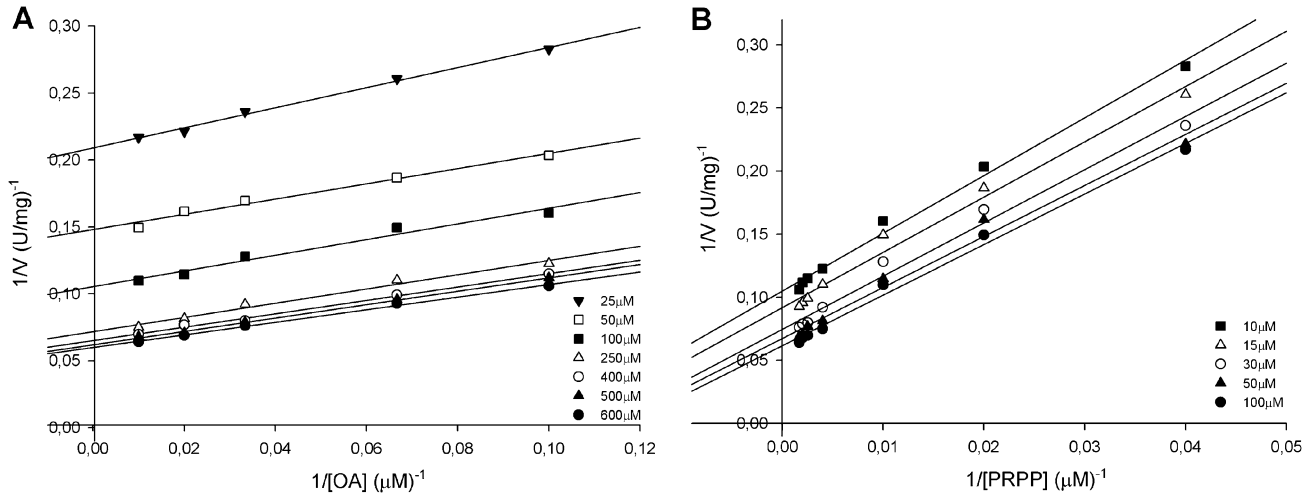

Fig. 2 Double reciprocal plots of the forward reaction of *Mt*OPRT. Steady-state initial velocity experiments were carried out as described in Experimental procedures. (A) Concentration of OA was varied (2–100 μM) in the presence of seven fixed different concentrations of PRPP. (B) Concentration of PRPP was varied (25–500 μM) in the presence of five fixed different concentrations of OA. Data were fitted to eqn (4).

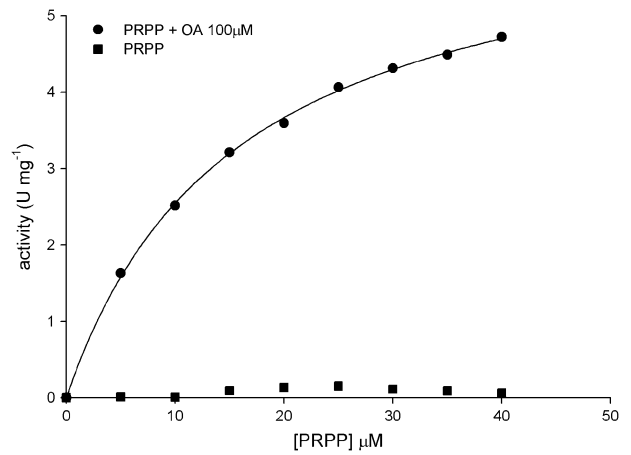

Fig. 3 Indirect PP_i release measurement by monitoring 2-amino-6-mercapto-7-methylpurine formation in the absence (■) and presence (●) of OA (100 μM) in the reaction mixture.

When varying PRPP (25–400 μM) and the product OMP (12–25 μM) at saturating concentration of OA (50 μM) or varying OMP (3–12 μM) at non-saturating concentration of OA (6 μM), mixed-type inhibitions were observed (Table 3, Fig. S1 of ESI‡). Similar results were observed when OA (6–75 μM) and the product PP_i (25–120 μM) were varied in the presence of both saturating (400 μM) and non-saturating (50 μM) concentrations of PRPP (Table 3, Fig. S2 of ESI‡). For varying concentrations of substrate OA (6–75 μM) and product OMP (24–60 μM) in the presence of saturating concentration of PRPP (400 μM) (Table 3, Fig. S1 of ESI‡), a noncompetitive inhibition profile was obtained. On the other hand, for varying concentrations of substrate OA (6–75 μM) and product OMP (6–25 μM) in the presence of non-saturating concentration of PRPP (50 μM) (Table 3, Fig. S1 of ESI‡), a mixed-type inhibition was observed instead. Variation of substrate PRPP (25–400 μM) and product PP_i (25–125 μM) in the presence of saturating OA concentration (50 μM) showed a noncompetitive inhibition pattern that changed to a mixed-type one when OA was fixed at a non-saturating concentration (6 μM) and fixed–varied PP_i concentration range was 25–75 μM (Table 3, and Fig. S2 of ESI‡). According to Rebholz and Northrop's studies on kinetics of Iso mechanisms,[28] the observed product inhibition pattern is in agreement with a Mono-Iso Ordered Bi–Bi kinetic mechanism (Fig. 4). It should be pointed out that isomerization of a stable enzyme form (Iso mechanism) does not affect the velocity equation in the absence of products, but the product inhibition patterns are changed. Values of α, constant that defines the degree to which substrate binding affects the affinity of the enzyme for an inhibitor, indicate whether a product inhibitor has higher affinity for free enzyme ($\alpha > 1$), or increased affinity for enzyme–substrate(s) complex(es) as compared to free enzyme ($0 < \alpha < 1$), or equal affinity for all enzyme forms ($\alpha = 1$).[29] Values of α were determined from fitting product inhibition data to eqn (5), and are shown in Table 3.

ITC ligand binding assays

As product inhibition data were consistent with a Mono-Iso Ordered Bi–Bi kinetic mechanism, substrate(s) and product(s) binding processes were assayed by ITC at 25 °C to ascertain the order of chemical compound addition. These binding assays showed that PRPP and OMP can bind to free *Mt*OPRT

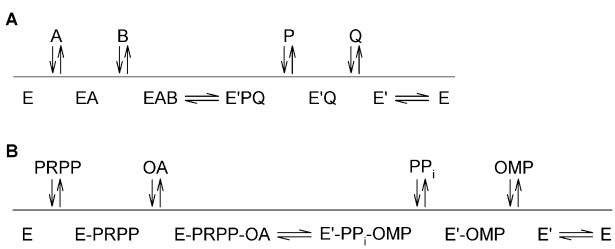

Fig. 4 (A) Kinetic mechanism of *Mt*OPRT as proposed by product inhibition assays. E and E′ correspond to enzyme isoforms. A and B, P and Q indicate substrates and products of the reaction. (B) Order of substrates binding and products released from *Mt*OPRT binding site, inferred from ITC ligand binding assays.

Table 3 Product inhibition results for *Mt*OPRT forward reaction

Inhibitor	Varied substrate	Fixed substrate	αK_i/μM	K_i/μM	α	Inhibition type[a]
OMP	PRPP	OA saturated	107 ± 85	10 ± 2	11	Mixed-type
		OA unsaturated	44 ± 15	4.4 ± 0.8	10	Mixed-type
	OA	PRPP saturated	35 ± 4	35 ± 10	1	Noncompetitive
		PRPP unsaturated	10.7 ± 0.4	7.4 ± 0.7	1.4	Mixed-type
PP_i	PRPP	OA saturated	108 ± 9	108 ± 19	1	Noncompetitive
		OA unsaturated	310 ± 53	26 ± 3	12	Mixed-type
	OA	PRPP saturated	120 ± 14	209 ± 97	0.6	Mixed-type
		PRPP unsaturated	145 ± 17	29 ± 4	5	Mixed-type

[a] In the W. W. Cleland nomenclature, mixed-type inhibitor patterns are called noncompetitive.

enzyme (Fig. 5A and B). ITC data on PRPP and OMP binding were fitted to, respectively, sequential binding sites and one set of site models (where the number of ligand sites was set to two for the sequential model). ITC data fitting yielded the thermodynamic constants ΔH and K_a, whereas ΔS and ΔG values were calculated using eqn (6), and K_d was calculated as the inverse of K_a (Table 4). The value near unity for the number of sites (N) given by ITC data fitting to one set of sites model for OMP suggests that there is one ligand molecule bound to each subunit of homodimeric *Mt*OPRT enzyme (Table 4). On the other hand, no binding to free *Mt*OPRT enzyme could be detected for OA and PP_i even when ligand concentrations were 600-fold and 900-fold larger than their K_M values (Fig. 5C and D). These results are in agreement with the Mono-Iso Ordered Bi–Bi kinetic mechanism in which PRPP binding to free enzyme is followed by OA binding to form a ternary complex, and PP_i product release is followed by OMP dissociation from a *Mt*OPRT:OMP binary complex to yield free enzyme (Fig. 4). The thermodynamic signatures of non-covalent interactions to each binding process indicate a net favorable (negative ΔH) enthalpy and unfavorable entropy (positive $-T\Delta S$ or negative ΔS) for both PRPP and OMP binding to *Mt*OPRT (Fig. 6).

ITC binding assays for dead-end complex formation

Results from product inhibition assays (Table 3) indicated values of $\alpha < 1$ when both OA and PP_i were varied in the presence of a fixed saturating PRPP concentration, suggesting that varied ligands show increased affinity for enzyme–substrate(s) complex(es) as compared to free enzyme. The possibility of both OA and PP_i being able to occupy, simultaneously, the enzyme's active site was assessed by ITC binding assays, in which OA was titrated into the *Mt*OPRT:PP_i complex and PP_i was titrated into the *Mt*OPRT:OA binary complex. ITC data on OA binding to the *Mt*OPRT:PP_i binary complex (Fig. 7A) and PP_i binding to the *Mt*OPRT:OA binary complex (Fig. 7B) clearly demonstrate that there is dead-end complex formation. These ITC data were fitted to a sequential binding model with the number of ligand sites set to 4 (Table 4—$PP_i{\cdot}OA_1$ and $PP_i{\cdot}OA_2$ corresponding to data derived from experiment depicted in Fig. 7A; $PP_i{\cdot}OA_3$ and $PP_i{\cdot}OA_4$ corresponding to data derived from experiment depicted in Fig. 7B). Thermodynamic discrimination profiles for *Mt*OPRT:PP_i:OA dead-end complex formation displayed two patterns (for each dead-end pair observed: $PP_i{\cdot}OA_1$ and $PP_i{\cdot}OA_2$ when OA was the titrated ligand; $PP_i{\cdot}OA_3$ and $PP_i{\cdot}OA_4$ when PP_i was the titrated ligand): one binding event driven by favorable enthalpy and unfavorable entropy, and a second binding event displaying unfavorable enthalpy and favorable entropy (Table 4).

Re-examination of the *Mt*OPRT enzyme mechanism

The steady-state kinetic data yielded a pattern of apparently parallel lines suggesting a Ping-Pong mechanism (Fig. 2), and the data were initially fitted to eqn (4). However, absence of PP_i release into solution in half-reaction measurements in the absence of OA, product inhibition patterns demonstrating a Mono-Iso Ordered Bi–Bi kinetic mechanism, and ITC measurements showing that PRPP and OMP can bind to free enzyme whereas OA and PP_i cannot, suggested that steady-state kinetic data should be re-examined. Accordingly, the steady-state kinetic data were fitted to eqn (7) for an Ordered Bi–Bi system, yielding similar values for the steady-state kinetic constants (Table 2).

Discussion

Amplification, cloning, expression and purification

DNA sequencing of *pyrE*-encoded *Mt*OPRT cloned into the pET-23a(+) expression vector revealed a silent mutation, which fortunately did not hamper further efforts. Interestingly, the size exclusion chromatography of the three-step purification protocol of recombinant *Mt*OPRT produced by *E. coli* host cells resulted in a decrease in the enzyme specific activity (Table 1). It has been reported that 40–50 mM of Na_2SO_4, $(NH_4)_2SO_4$ and K_2HPO_4 inhibit *E. coli* OPRT enzyme activity, whereas NaCl at a concentration up to 200 mM showed no inhibitory effect on the enzyme's activity.[30] It is thus puzzling that NaCl salt removal of *Mt*OPRT by size exclusion chromatography lowered the enzyme activity. Notwithstanding, this reduction in *Mt*OPRT activity was reverted after elution at approximately 660 mM $(NH_4)_2SO_4$ from the hydrophobic interaction column. Although the purification protocol described here involves three chromatographic steps, this protocol yielded ~64% of homogeneous *Mt*OPRT protein, which is approximately 3 times larger than a single-step OMP column affinity[31] and Ni^{2+} affinity purification protocols published for OPRT homologues.[14,32] Homogeneous recombinant *Mt*OPRT was dialyzed against buffer A to remove $(NH_4)_2SO_4$, and stored up to 12 months at −80 °C in the presence of 5% glycerol with no loss of enzyme activity. As described for the yeast and *Plasmodium falciparum* homologues,[33,34] significant activity loss was observed when the enzyme was stored at 4 °C,

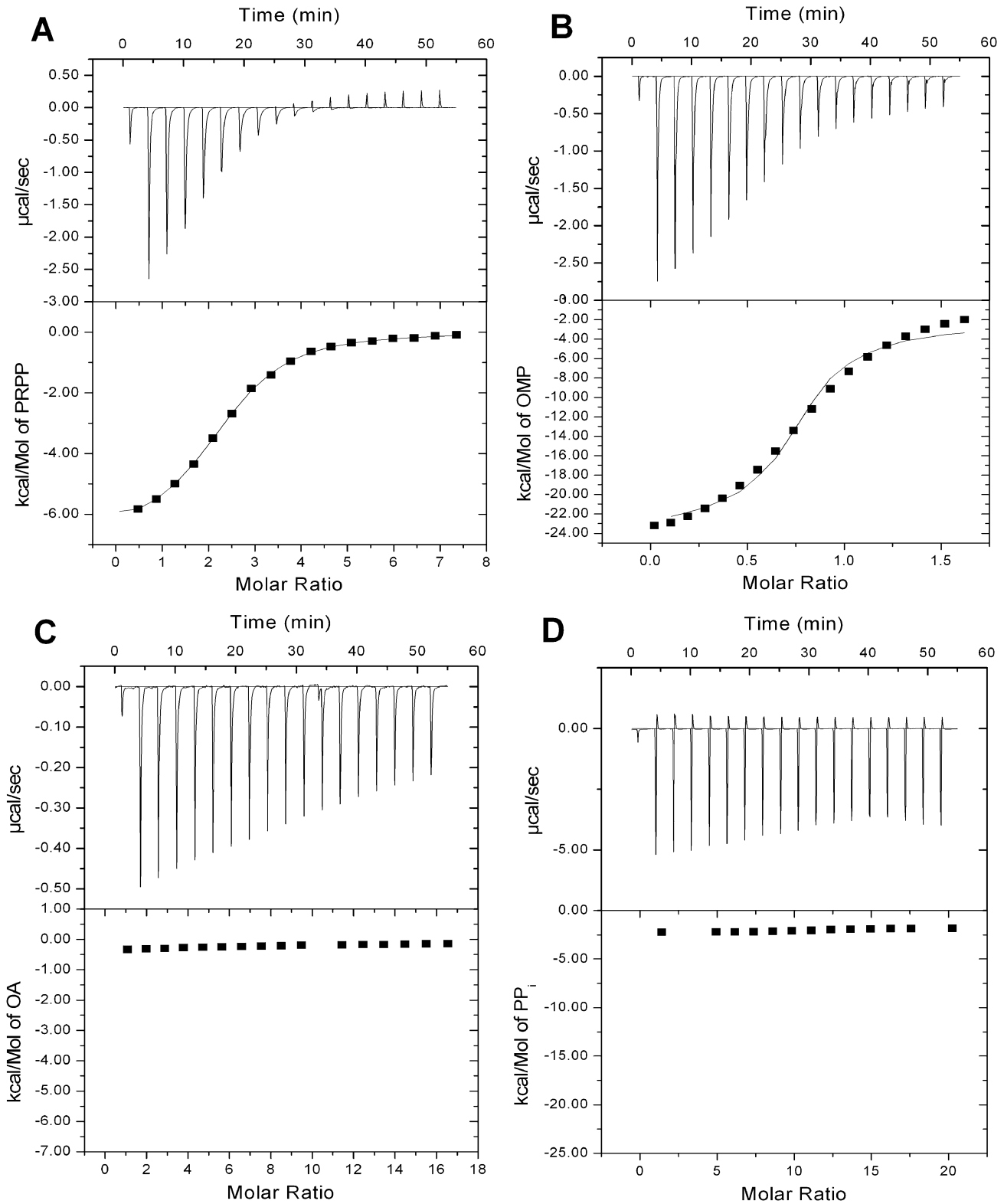

Fig. 5 Ligand binding assays. PRPP (A) and OMP (B) ITC data were fitted to sequential binding and one set of sites binding models. Both OA (C) and PP_i (D) binding to *Mt*OPRT apo form could not be detected under experimental settings.

with a half-life of 24 hours. The specific activity of OPRTs from *Saccharomyces cerevisiae*, *Rhizobium leguminosarum*, *Salmonella typhimurium* and *E. coli* was reported to be, respectively, 40 U mg^{-1},[35] 53 U mg^{-1},[32] 70–85 U mg^{-1},[24,36] and 400 U mg^{-1}.[37] A value of 105 U mg^{-1} for *Mt*OPRT specific activity is reported here.

Table 4 Thermodynamic, ligand binding affinity and dissociation constants; and number of ligands per subunit (N) for *Mt*OPRT

	ΔH/cal mol^{-1}	$-T\Delta S$/cal mol^{-1} degree^{-1}	ΔG/cal mol^{-1}	K_a/M^{-1}	K_d/μM	N
$PRPP_1$	−8.6 (±0.3) × 10^3	2.7 (±0.1) × 10^3	−6 (±0.2) × 10^3	20 (±2) × 10^3	52 (±5)	—
$PRPP_2$	−6.3 ± (0.4) × 10^3	0.37 (±0.02) × 10^3	−6 (±0.3) × 10^3	21 (±1) × 10^3	48 (±2)	—
OMP	−25.7 (±0.9) × 10^3	19 (±0.6) × 10^3	−7 (±0.2) × 10^3	124 (±2) × 10^3	8 (±1)	0.82 (±0.02)
$PP_i{\cdot}OA_1$	−43 (±2) × 10^3	37 (±2) × 10^3	−6 (±0.3) × 10^3	13 (±2) × 10^3	75 (±11)	—
$PP_i{\cdot}OA_2$	55 (±4) × 10^3	−60 (± 4) × 10^3	−5 (±0.3) × 10^3	4 (±0.6) × 10^3	261 (±41)	—
$PP_i{\cdot}OA_3$	13.1 (±0.5) × 10^3	−20 (±0.8) × 10^3	−7 (±0.3) × 10^3	127 (±20) × 10^3	8 (±1)	—
$PP_i{\cdot}OA_4$	−43 (±9) × 10^3	36 (±7) × 10^3	−6 (±1) × 10^3	58 (±9) × 10^3	17 (±2)	—

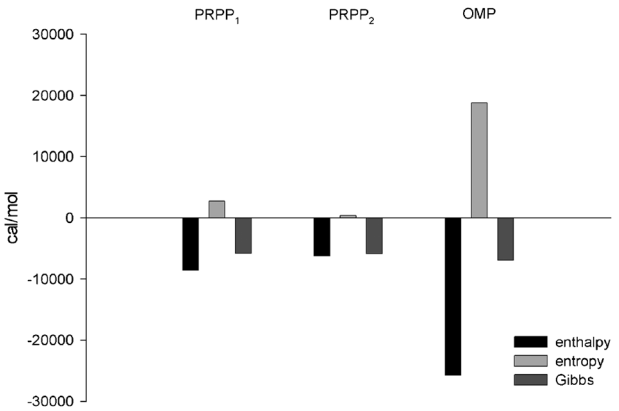

Fig. 6 Enthalpy (ΔH), entropy ($-T\Delta S$) and Gibbs free energy (ΔG) thermodynamic profile for PRPP and OMP binding to *Mt*OPRT. As ITC data on PRPP binding were fitted to a sequential binding sites model, values are also given for each binding site of homodimeric *Mt*OPRT (PRPP 1 and PRPP 2).

Mass spectrometry identification and molecular mass determination

Mass spectrometry data indicated a value of 18 761 Da for subunit molecular mass of *Mt*OPRT, which is in agreement with the theoretical value for the 179 amino acids of its primary sequence. 'Type I PRTases' (phosphoribosyltransferases), which are involved in nucleotide synthesis or salvage pathways, are known to present remarkable tertiary and quaternary structure conservation[25,38] regardless of the conservation of their primary structure. Exception to the observed high variation in the amino acid sequence is a conserved PRPP binding motif of 13 amino acids, shared with the PRPP synthases,[39] being the main unifying characteristic of the primary structure for this group of enzymes.[12] The PRPP binding motif is conserved in the *Mt*OPRT primary sequence, comprising amino acids 116 to 128 (VLVVEDTSTTGNS—Fig. 8, underlined), as well as an 11-amino acid long conserved flexible loop (amino acids 94 to 104—RKSAKAHGMQR, Fig. 8, shaded in gray) involved in

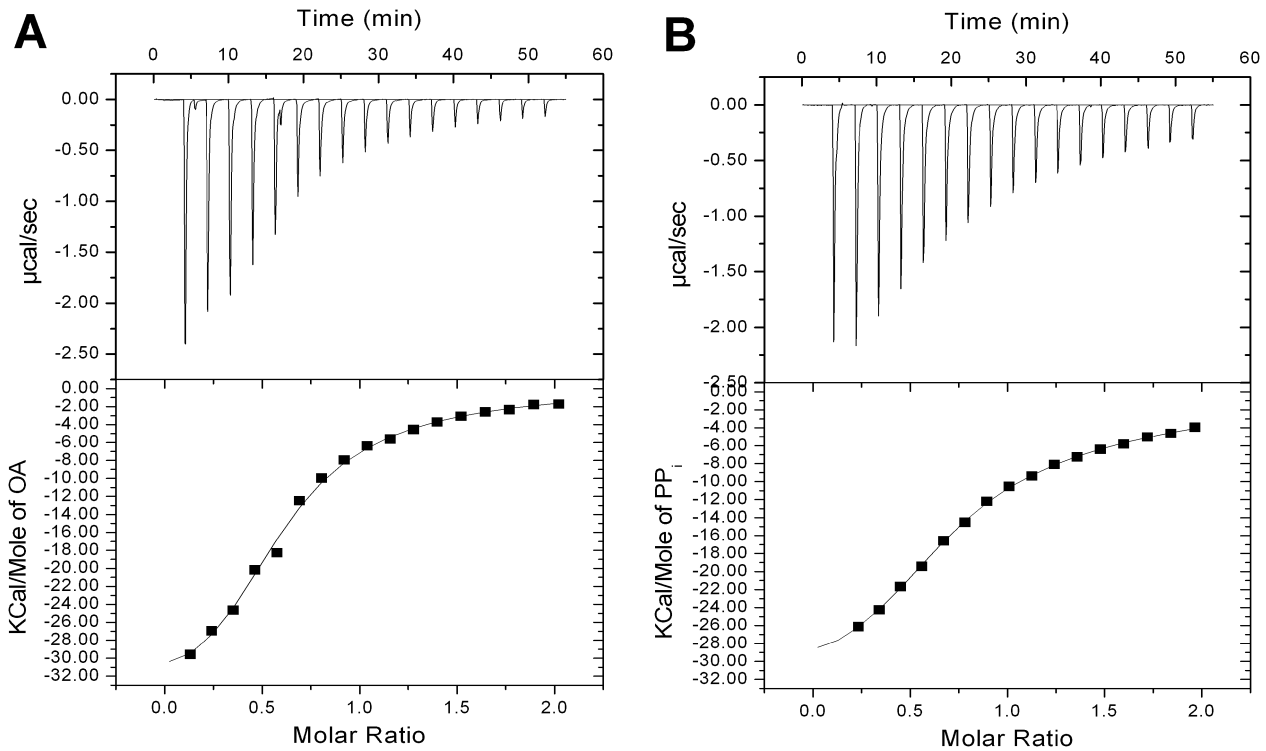

Fig. 7 Dead-end complex formation of product PP_i and substrate OA with *Mt*OPRT. (A) Incubation of enzyme and PP_i, titration of OA; (B) incubation of enzyme and OA, titration of PP_i.

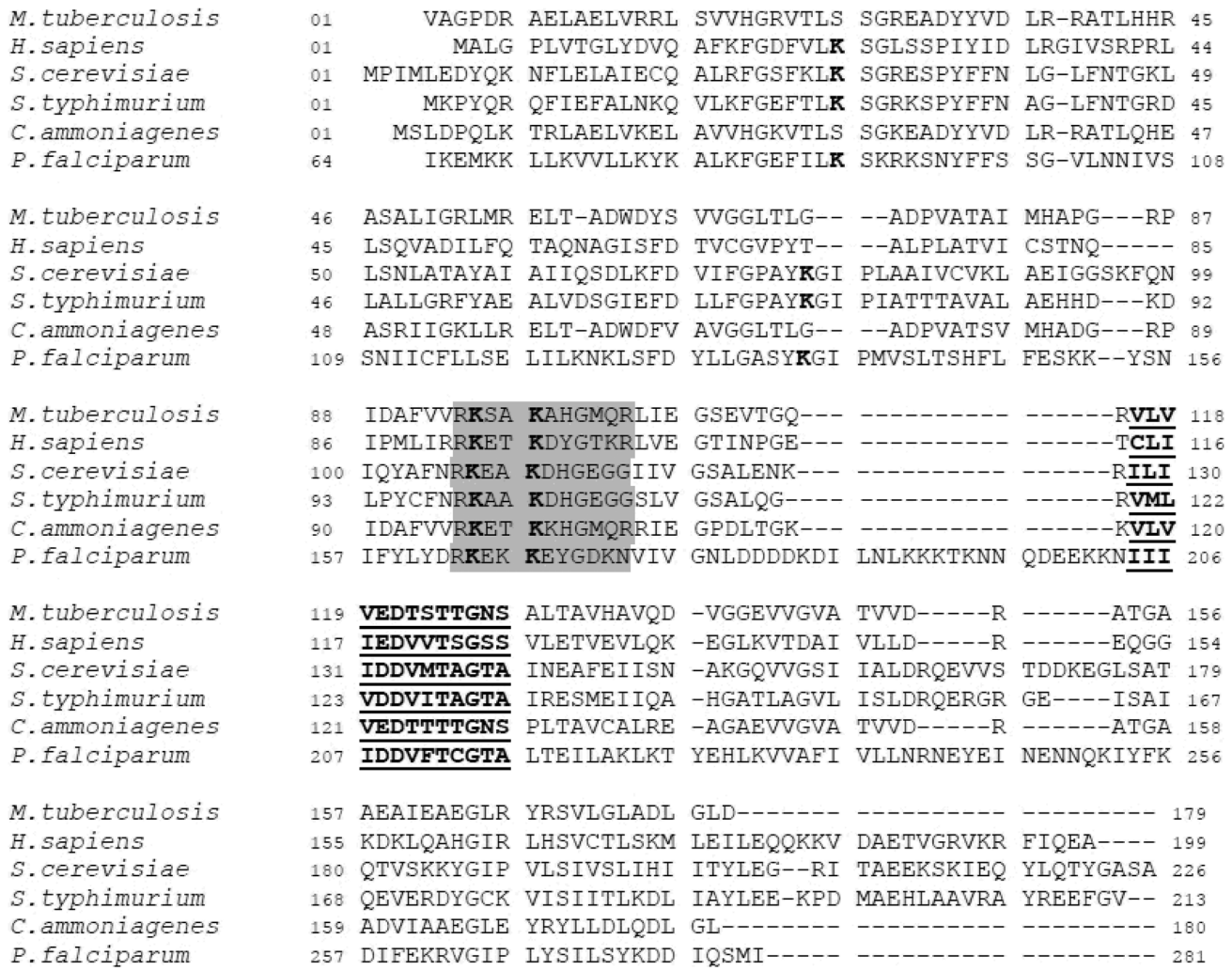

Fig. 8 Neighbor-joining multi sequence alignment of MTB (TubercuList: Rv0382c), *H. sapiens* (GenBank: NP_000364.1), *S. cerevisiae* (UniProt: P13298), *S. typhimurium* (GenBank: NP_462633), *C. ammoniagenes* (GenBank: EU123869) and *P. falciparum* (GenBank: XP_001351684) OPRT enzymes, performed with ClustalW.[72] In *P. falciparum* first 63 amino acids were omitted from sequence alignment. Conserved catalytic lysine residues, and amino acids comprising the catalytic loop and the PRPP binding site are highlighted in bold, shaded in gray and underlined respectively.

PRPP substrate binding and partial exclusion of the solvent from the enzyme active site.[30,38,40–42] Another shared feature of Type I PRTases is the catalytic role of conserved lysine residues (Fig. 8, bold)[43,44] involved in the binding of a highly charged Mg^{2+}:PRPP complex and anionic form of OA at pH 8.0.

Analytical HPLC gel filtration

As Type I PRTases are homodimeric,[39] size exclusion results presented here showing that *Mt*OPRT is a homodimer of approximately 38 kDa in solution suggest that it belongs to Type I PRTases. OPRTs from other organisms have also been shown to be homodimers[24,32,35,37,45] including *P. falciparum*.[14] However, the latter was shown to be expressed as a 140 kDa enzyme complex containing two OPRT subunits and two OMP decarboxylase subunits.[46] Although encoded by separate genes, and capable of catalyzing individual reactions, tetramer assembly seems to enhance *P. falciparum* OPRT and OMP decarboxylase activities and stability.[47] Crystallographic structures determination indicated that loop closure upon substrate binding occurs between adjacent subunits, locating OPRTs two active sites at such interfaces, indicating that the catalytic lysine residue in the loop (*Mt*OPRT Lys98) actually plays this role in the active site of the adjacent subunit.[30,38,40–42,48–51] OPRT active sites are thus formed by amino acids of both subunits, and the homodimeric quaternary structure corresponds to the biologically active form. The key role of this lysine residue (Lys98 in *Mt*OPRT) might explain its conservation in OPRTs (Fig. 8).

Comparison of steady-state kinetic parameters

Divalent metal ion activation of substrate PRPP has already been demonstrated as essential for phosphoribosyltransferase-catalyzed reactions,[35] in which the binary 1 : 1 Mg^{2+}·PRPP complex was proved to be the true substrate for OPRT reaction.[36] Although *S. typhimurium* OPRT has been shown to have a residual activity of 1 U mg^{-1} in the absence of Mg^{2+},[36] no activity could be detected when Mg^{2+} was omitted from the reaction mixture for the *Mt*OPRT (data not shown). The latter indicates that Mg^{2+}:PRPP

is the true substrate for *Mt*OPRT, in agreement with Type I PRTases.[39] The set of *Mt*OPRT kinetic constants listed in Table 2 showed an approximately 10-fold larger value for the overall dissociation constant (K_M) of PRPP as compared to OA for the forward reaction, and an approximately 6-fold larger K_M value for PP_i in comparison to OMP for the reverse reaction. Higher overall dissociation constants values for PRPP than for OA have also been reported for *P. falciparum* (1.5-fold)[14] and *C. ammoniagenes* (2-fold).[26] In addition, OMP appears to be the preferred substrate for the reverse reaction for *S. typhimurium*[24,25] and *S. cerevisiae* homologues.[23] *Mt*OPRT presents larger K_M values as compared to the human homologue (Table 2). However, human OPRT is a bifunctional enzyme encoded by a single gene (*pyr5*, GenBank ID: NP_000364.1) whose N-terminal portion has OPRT activity while the C-terminal portion presents OMP decarboxylase activity.[27] Accordingly, the K_M values for OA and OMP substrates of human OPRT (Table 2) actually correspond to, respectively, OPRT and OMP decarboxylase portions, and not directly to the reversal of phosphoribosyltransferase reaction. In addition to the ligands given in Table 2, *P. falciparum*,[14] *S. typhimurium*[36] and human[25] homologues have been shown to also employ, respectively, 5-fluororotate, uracil and 5-fluoruracil as alternative substrates. However, *Mt*OPRT showed no activity towards uracil or 5-fluoruracil (data not shown). The $k_{catforward}/k_{catreverse}$ ratio indicates that the forward reaction is faster than the reverse reaction for *Mt*OPRT. The k_{cat} value for *Mt*OPRT demonstrates low catalytic efficiency in comparison to *P. falciparum*,[14] *S. cerevisiae*[23] and *Homo sapiens*[27] homologues (Table 2). A possible explanation is that active site lysine residues that play catalytic roles (Lys26 and Lys73 in *S. typhimurium*)[43,44,48] are replaced with Ser26 and Gly72 in *Mt*OPRT, thereby reducing the catalytic constant of the latter. Notwithstanding, site-directed mutagenesis efforts should be pursued to lend or not support to this proposal.

Steady-state kinetics

Double reciprocal patterns of apparently parallel lines for forward reaction (Fig. 2) is an indication that the reaction catalyzed by *Mt*OPRT obeys a double-displacement or Ping-Pong kinetic mechanism, in which the binding of the first substrate is followed by the release of the first product prior to second substrate binding to the active site. Nonetheless, sequential mechanisms have been suggested as one of the characteristics of Type I PRTases,[14,25,39] where the sole exception was *S. cerevisiae* OPRT, for it a Ping-Pong was initially attributed.[35] However, it was subsequently shown that *S. cerevisiae* OPRT follows a sequential mechanism,[52] most likely a Theorell–Chance variant.[23] To try to address this issue, the experiments described below were pursued.

Half-reaction detection of PP_i release in solution

In bi-substrate reaction in which a portion of a molecule is transferred to a second one, the donor molecule usually binds first and transfers to the enzyme active site a molecular group.[29] In case the PRPP substrate binds first and transfers its 5′-phosphate ribose moiety to *Mt*OPRT enzyme active site prior to OA binding to form OMP by two separated half-reactions (E + PRPP → E:Prib + PP_i, and E:Prib + OA → E + OMP), the release of PP_i into solution should be detectable in the absence of OA. Fig. 3 shows that release of PP_i by the reaction catalyzed by *Mt*OPRT can only be detected in the presence of OA, thereby ruling out a Ping-Pong mechanism in which PRPP would transfer the 5′-phosphate ribose moiety to the enzyme. In addition, there are some conditions where lines seem to be parallel and indicate Ping-Pong mechanisms,[53,54] but in reality are sequential mechanisms that can be distinguished by a complete set of product inhibition experiments.[28,55]

Enzymatic reaction mechanism determination by product inhibition assays

Product inhibition results (Table 3) are consistent with a Mono-Iso Ordered Bi–Bi kinetic mechanism (Fig. 4A).[28,56] Although product inhibition results allow identification of substrate–product pairs (PRPP and PP_i, OA and OMP); they do not unambiguously indicate the order of substrate addition and product release, as the inhibition patterns are symmetrical.[53,55] The Mono-Iso Ordered Bi–Bi kinetic mechanism implies that *Mt*OPRT undergoes an isomerization of the transitory ternary complex formed upon binding of substrates prior to release of products, and the "product" form of free enzyme has to isomerize back to the "substrate" form.[57] Enzymes that isomerize slowly enough to influence the rate of catalytic turnovers are said to have "Iso mechanisms".[28] Based on steady-state kinetics data and product inhibition studies a fractional reduction of the maximal velocity (f_{iso} = the average impact of the isomerization on the maximal velocities of the reaction in the forward and reverse directions together) can be estimated by the following equation: $f_{iso} = (K_{is}/K_{ii})/[(V_{reverse}/V_{forward}) + 1]$.[28] The value of f_{iso} will range from zero, when an Iso mechanism is insignificant, to one, when the isomerization is rate limiting.[28] Fitting the steady-state kinetics data (Table 2) and product inhibition data (Table 3) to this equation yielded ambiguous results. For instance, a value of 1.2 was estimated for f_{iso} at fixed-saturating PRPP substrate concentration and varied OA in the presence of PP_i product. On the other hand, a value of 0.06 was estimated at fixed-unsaturated OA concentration and varied PRPP concentration in the presence of PP_i product. Solvent-exposed loop closure during catalysis has been proposed to shield the active site of *S. typhimurium* OPRT,[25] as well as for other PRTases,[12,39] and was corroborated by crystallographic structure determination of *S. typhimurium* in the presence of ligands.[48,50] Loop closure of *S. typhimurium* OPRT has also been proposed to be essential for transition-state stabilization during phosphoribosyl group transfer and to shield the transition state from bulk solvent, accompanied by a partially rate-limiting loop opening after substrate to product conversion.[38]

ITC ligand binding assays

ITC measurements were carried out to both determine the order, if any, of addition of substrate and the order of product release to yield free enzyme. Formation of *Mt*OPRT:PRPP and *Mt*OPRT:OMP binary complexes (Fig. 5A and B) was detected by ITC measurements, whereas no binding of

either OA or PP_i to free *Mt*OPRT (Fig. 5C and D) could be detected. Notwithstanding, an enthalpy variation of 0.2 kcal mol^{-1} and 0.35 kcal mol^{-1} for, respectively, OA and PP_i, and hyperbolic-like profiles (if graphic axis was adjusted to fit scale in Fig. 5C and D) might indicate that larger concentrations, solubility permitting, of OA and PP_i may bind to free *Mt*OPRT. However, it is unlikely to be relevant in the intracellular context.

ITC data on PRPP binding to free *Mt*OPRT were best fitted to a sequential binding sites model, with the *n* value (number of active sites) fixed as two (in agreement with the homo-dimeric quaternary structure), yielding the values given in Table 4 and depicted in Fig. 6 for each independent PRPP binding event. ITC data on PRPP binding to free *Mt*OPRT were best fitted to a sequential binding sites model, yielding the values given in Table 4 and depicted in Fig. 6. It is noteworthy that binding of the first PRPP molecule appears to trigger large conformational changes likely in *Mt*OPRT protein upon binary complex formation as suggested by the entropically unfavorable (negative ΔS) contribution of non-covalent interactions to the binding process.[58] Binding of the second PRPP molecule is accompanied by smaller unfavorable entropic contribution. At any rate, there appears to be enthalpy–entropy compensation as ΔG values are similar[59,60] (Table 4).

ITC data on OMP binding to free *Mt*OPRT were best fitted to one set of sites binding model, indicating that one molecule of OMP binds to each enzyme active site (1 : 1 stoichiometry) with equal affinity (Table 4 and Fig. 6). These results corroborate the Mono-Iso Ordered Bi–Bi kinetic mechanism, where PRPP binds to *Mt*OPRT first followed by OA binding, there occurs an enzyme conformational change, and PP_i is the first product to dissociate followed by OMP release to yield the "product" form of free enzyme that has to isomerize back to the "substrate" form (Fig. 4B). Movements of the flexible loop appear to be integral to catalysis of Type I PRTases, both covering the active site and recruiting essential residues to the catalytic locus.[25] Accordingly, PRPP and OMP binding to *Mt*OPRT are enthalpy-driven processes with negative values for Gibbs energy changes demonstrating that these binding events are favorable and accompanied by an unfavorable entropy contribution that likely reflects enzyme's loop closure. The larger ΔH value for OMP as compared to PRPP is probably due to more H bonds and hydrophobic contacts of the former with the enzyme's active site, as indicated by crystallographic data available.[42]

Dead-end complex formation

A calculated value of 0.6 for α from product inhibition data suggests that when the substrate PP_i is varied along with OA in the presence of a fixed-saturating concentration of PRPP (Table 3), PP_i has higher affinity for enzyme forms other than free *Mt*OPRT; suggesting that PP_i and OA can both occupy the enzyme's active site simultaneously in a dead-end complex. ITC ligand binding assays confirmed that OA can bind to *Mt*OPRT in the presence of saturating PP_i concentration (900 μM; Fig. 7A), and that PP_i can bind to *Mt*OPRT in the presence of saturating OA concentration (800 μM; Fig. 7B).

Although the ITC results clearly showed *Mt*OPRT:PP_i:OA ternary complex formation according to a sequential binding sites model, how can one reconcile *Mt*OPRT:PP_i:OA abortive complex formation with lack of enzyme–ligand binary complex formation? The abortive complex (*Mt*OPRT:PP_i:OA) formation has been supported by isotopic exchange and equilibrium binding assays of *S. typhimurium* OPRT that showed stronger PP_i binding to OPRT enzyme in the presence of OA as compared to weak binding of PP_i to free enzyme.[25,38] Presence of both PP_i and OA, in the absence of PRPP and OMP, might result in a synergic positive cooperative binding.[59] However, whether or not formation of the *Mt*OPRT:PP_i:OA abortive complex is relevant in the intracellular context is yet not known. Although a site other than the active site that can bind either OA or PP_i could be invoked, the ITC data were best fitted to a sequential binding model with the number of ligand sites set to 4. However, it could be speculated that for the reverse reaction binding of the OA moiety of OMP could result in conformational changes that increase PP_i binding. A *Mt*OPRT:PPRPP:OMP dead-end complex is not expected to form because of overlapping chemical groups in the enzyme active site.[55] Data presented in Table 4 show that the four binding events of two PP_i and two OA molecules all have similar ΔG values, an indication of enthalpy–entropy compensation.[59,60]

Proposal of the *Mt*OPRT enzyme mechanism that is consistent with kinetic and thermodynamic data

Although the pattern of apparently parallel lines in double reciprocal plots (Fig. 2) suggested a Ping-Pong mechanism, half-reaction measurements, product inhibition and ITC data do not lend support to this mechanism. Similarly, *S. cerevisiae* OPRT was initially suggested to follow a Ping-Pong mechanism,[35] which was later shown to follow a sequential mechanism.[52] These discrepancies prompted us to re-evaluate the steady-state kinetic data, which were thus fitted to eqn (7) for an Ordered Bi–Bi system. The values for the steady-state kinetic constants are similar whether fitting the data to a Ping-Pong mechanism or to an Ordered Bi–Bi system (Table 2). There are some conditions where parallel lines in double-reciprocal plots are not truly so. For instance; a family of reciprocal plots for an Ordered Bi–Bi system the K_{ia} value of which is much smaller than K_a would appear to be parallel as they intersect far to the left of the $1/v$ axis and far below the $1/[S]$ axis.[53] The $K_{ia}K_b$ term of eqn (7) would thus tend to zero, and this equation would be reduced to eqn (4). Fitting the steady-state kinetic data to eqn (7) yielded values of 0.75 μM for K_{ia} (PRPP) and 96 μM for K_a (Table 2), which is in agreement with an ordered mechanism with a pattern of apparently parallel lines in double-reciprocal plots (Fig. 2).

Conclusion

Currently anti-TB available drugs are considered not completely efficacious[61] due to natural and emerging disease characteristics that might impose some obstacles to its treatment.[62] TB control and eradication thus require the identification of novel molecular targets for the rational design of inhibitors and development of novel treatments to improve patient compliance.[2,17]

The target-based rational design of new agents with anti-TB activity includes functional and structural efforts. Accordingly, mechanistic analysis should be included in enzyme-targeted drug programs aiming at the rational design of potent enzyme inhibitors.[12] *Mt*OPRT appears to be a promising drug target as DNA metabolism is maintained in both active and latent forms of TB, and the *de novo* pyrimidine synthesis has been shown to be essential for mycobacterial survival.[21] As a Type I PRTase, the *Mt*OPRT homodimeric quaternary structure, and conservation of the primary structure of the PRPP binding site and the catalytic loop were not surprising results. These findings will most likely reflect on *Mt*OPRT three-dimensional structure, as Type I PRTases are known for their tertiary and quaternary structure resemblance. Notwithstanding, here we propose a novel Mono-Iso Ordered Bi–Bi kinetic mechanism for *Mt*OPRT, which is supported by steady-state kinetics, product inhibition, ITC assays and half-reaction measurements. The slow conformational change of the "product" form of free enzyme to the "substrate" form (Iso segment after product release) is in agreement with the low k_{cat} value for *Mt*OPRT, which is a characteristic of Iso mechanisms.[28] The Mono-Iso Ordered Bi–Bi mechanism can be exploited in the rational design of *Mt*OPRT enzyme inhibitors. For instance, a chemical compound that locks the *Mt*OPRT enzyme in the "product" form will likely impede (or slow down) binding of the first substrate (PRPP) and thereby inhibit the enzyme activity. Interestingly, dynamic features of conformational changes (non-chemical steps) of *Cryptosporidium parvum* inosine monophosphate dehydrogenase (IMPDH) have been exploited to design parasite-specific inhibitors of IMPDH enzyme activity.[63] In addition, the *Mt*OPRT:PP_i:OA dead-end ternary complex formation could also be employed in the planning of *Mt*OPRT enzyme inhibitors based on, for instance, the fragment approach.

Understanding the mode of action of *Mt*OPRT may be useful to chemical biologists interested in designing function-based chemical compounds to elucidate the biological role of this enzyme in the context of whole MTB cells. Efforts towards understanding *Mt*OPRT function under cell-like dense conditions are also worth pursuing as it has been shown that molecular crowding can affect protein structure, stability, function and activity.[64] Moreover, attempts to ascertain the role of *Mt*OPRT in MTB survival *in vivo* during both active and latent TB are currently ongoing. At any rate, the data on *Mt*OPRT mode of action presented here provide a solid foundation on which to base the development of inhibitors of *Mt*OPRT enzyme activity.

Experimental procedures

Gene amplification

The *pyrE* gene (Rv0382c) was PCR amplified from total genomic DNA of MTB H37Rv strain using specific primers designed to contain *Nde*I (primer sense 5′gaa**catatg**gccgg-acctgaccgcgcagagttggc3′) and *Hind*III (primer antisense 5′gc**aagctt**ctaatccagccccagatcggccaggcc3′) restriction sites (highlighted in bold). PCR cycling parameters were 35 cycles of denaturation at 98 °C (30 s), annealing at 55 °C (45 s) and extension at 72 °C (2 min). The PCR product was visualized on 1% agarose gel and purified from the gel using a QIAGEN QIAquick gel extraction kit. The purified fragment was initially cloned into pCR-Blunt vector (Invitrogen) and subcloned into pET-23a(+) expression vector (Novagen), previously digested with *Nde*I and *Hind*III restriction enzymes. The integrity of constructs was confirmed in all cases by appropriate selections and digests with appropriated restriction enzymes (New England Biolabs). Inserted sequences were confirmed by DNA sequencing in all cases.

Recombinant protein expression, purification and molar absorption coefficient determination

Competent *E. coli* BL21(DE3) cells were electroporated with pET-23a(+)::*pyrE* recombinant vector. Cells were grown overnight at 37 °C and 180 rpm in 100 mL Luria-Bertani (LB) medium containing ampicillin 50 μg mL^{-1}. A volume of 13 mL of this culture was used to inoculate 500 mL LB medium supplemented with ampicillin (50 μg mL^{-1}), grown at 37 °C and 180 rpm to an optical density (OD_{600nm}) of 0.4, and induced with 1 mM IPTG. Cells were harvested by centrifugation (8000 *g*) for 12 h after induction, at 4 °C and immediately submitted to purification protocol steps. All protein purification steps were performed at 4 °C or on ice. Chromatographic steps were performed by High-Performance Liquid Chromatography (HPLC) on an Äkta Purifier System (GE HealthCare). Cell pellet (12 g) was suspended in 60 mL of buffer A (Tris HCl 50 mM pH 8.0) and stirred for 30 min. Lysozyme (Sigma Aldrich) was added to a final concentration of 0.2 mg mL^{-1} and incubated for 30 min under constant stirring. The mixture was sonicated (15 pulses of 10 s, spaced by 1 min), the lysate was centrifuged for 30 min at 48 000 *g*. Streptomycin sulfate (Sigma Aldrich) was added to the supernatant to a final concentration of 1%, centrifuged for 30 min at 48 000 *g*. The supernatant was dialyzed against buffer A (2 times against 2 L for 3 h each, and a third time against 2 L overnight), and clarified by centrifugation at 48 000 *g* for 30 min. The supernatant was loaded on an anionic exchange chromatographic column (HiPrep Q-XL 16/10, GE Health-Care) equilibrated with buffer A, washed with 8 column volumes (CV) of buffer A, followed by 20 CV of 0–70% linear gradient of buffer B (Tris HCl 50 mM, NaCl 500 mM, pH 8.0) at 1 mL min^{-1} flow rate. Fractions containing the recombinant enzyme, as inferred by 12% SDS-PAGE polyacrylamide electrophoresis stained with Coomassie Blue, were pooled, concentrated to a final volume of 9 mL using a 50 mL stirred ultrafiltration cell (Millipore) with a 10 kDa cutoff filter. The concentrated recombinant protein was loaded into a size exclusion chromatographic column (HiPrep 26/60 Sephacryl S200 HR, GE HealthCare) equilibrated with buffer A. Proteins were eluted under isocratic conditions with 1 CV of buffer A at 0.2 mL min^{-1} flow rate. Fractions containing *Mt*OPRT were treated with Tris HCl 50 mM, $(NH_4)_2SO_4$ 2 M, pH 8.0 to a final concentration of Tris HCl 50 mM, $(NH_4)_2SO_4$ 1 M, pH 8.0 (buffer C), under constant stirring for 30 min, and centrifuged for 30 min at 48 000 *g*. The supernatant was then loaded on a hydrophobic interaction chromatographic column (HiLoad 16/10 Phenyl Sepharose HP, GE HealthCare)

equilibrated with buffer C. The hydrophobic interaction column was washed with 10 CV of buffer C and the homogeneous recombinant *Mt*OPRT was eluted using a 20 CV linear gradient of 0–65% of buffer A, at a 1 mL min^{-1} flow rate. Eluted fractions containing homogeneous *Mt*OPRT were dialyzed against 2 L buffer A for 2 h, concentrated to 1 mg mL^{-1} and stored at −80 °C in 5% glycerol. Under these conditions *Mt*OPRT is stable up to 12 months. Protein concentration was determined either by the method of Bradford[65] or by direct absorbance measurement. A value of 11 570 $M^{-1}cm^{-1}$ was determined by the method of Edelhoch[66,67] for the molar absorption coefficient at 280 nm ($\varepsilon_{280\ nm}$) of *Mt*OPRT in buffer A.

Identification of *Mt*OPRT by mass spectrometry

Gel electrophoresis and staining. Samples containing *Mt*OPRT were mixed with sample loading buffer (Laemmli loading dye[68]) at a 1 : 1 final volume before loading onto 12% SDS-PAGE polyacrylamide gel and submitted to vertical electrophoresis at 120 V for 1 h. For protein staining, gels were fixed with Coomassie Blue for 20 min and destained with 10% acetic acid/25% methanol until the background was clear. Gel cutting was performed manually with a sterile scalpel.

In-gel digestion. In-gel digestion was performed according to that reported by Shevchenko.[69] Briefly, an excised gel band corresponding to *Mt*OPRT was cut into small pieces and destained in 25 mM NH_4HCO_3 and 50% acetonitrile, dehydrated with acetonitrile, and dried. Gel pieces were then rehydrated with 12.5 ng μL^{-1} trypsin solution (in 25 mM NH_4HCO_3) and incubated overnight at 37 °C. Peptides were extracted twice with a solution containing 5% formic acid and 50% acetonitrile followed by a final extraction with acetonitrile. Samples were dried with a speed-vacuum centrifugation before analysis.

Mass spectrometry (MS). Tryptic digest of *Mt*OPRT was separated on a homemade column (solid phase Kinetex C18 of 2.6 μm particles, 0.1 × 1000 mm) using a nanoUPLC (nanoLC Ultra 1D plus, Eksigent, USA) and eluted directly to a nanospray ion source connected to a hybrid mass spectrometer (LTQ-XL and LTQ Orbitrap Discovery, Thermo, USA). The flow rate was set to 1 μL min^{-1} and the mass spectrometer was set to acquire one MS survey scan for the m/z range of 400–2000 (30 000 resolution) and MS/MS spectra for the ten most intense ions from the survey scan during the gradient. An isolation mass window of 15 ppm was used for the precursor ion selection, and the normalized collision energy value of 35% was used for fragmentation. Dynamic exclusion lasting for 30 s was used to acquire MS/MS spectra from low intensity ions. In MS survey, the preview mode for FTMS master scan was turned on, and only doubly and triply charged ions were selected for MS/MS. LC-MS/MS data were processed with Proteome Discoverer 1.0 (Thermo, USA) for comparison of MS/MS spectra with theoretical spectra generated from *in silico* tryptic digestion of MTB H37Rv proteome (downloaded from ftp://ftp.ncbi.nih.gov/genomes/). The search parameters were as follows: trypsin digestion, two missed cleavage allowance, carbamidomethylation on cysteine, variable oxidation on methionine, precursor tolerance of 10 ppm, and fragment tolerance of 0.8 Da. To exclude false identifications, only matches with XCore > 2.0 for doubly charged peptides and XCore > 2.5 for triply charged peptides were accepted.

Determination of *Mt*OPRT molecular mass

The homogeneous *Mt*OPRT was processed for removal of salts using homemade Poros 50 R2 (Applied Biosystems, USA) reverse phase tips, reconstituted in ACN 50%/FA 0.1% and loaded on an offline emitter (PicoTip Econotip, New Objective, Woburn, MA, USA). The emitter was submitted to electrospray ionization on a nanospray ion source (settings: source voltage 1.8 kV, capillary temperature 200 °C, capillary voltage 9 V, tube lens voltage 125 V) and averaged spectra were collected during 1 min on a Thermo Orbitrap Discovery XL. The average spectrum was processed with the software MagTran[70] for charge state deconvolution.

Analytical HPLC gel filtration

Determination of *Mt*OPRT molecular mass in solution was performed using a Superdex 200 HR 10/30 size exclusion column (GE HealthCare) at 0.4 mL min^{-1} flow rate and isocratic elution with 1 CV of Tris HCl 50 mM, NaCl 200 mM, pH 7.5. Proteins were detected at 215, 254 and 280 nm. The LMW and HMW Gel Filtration Calibration Kits (GE Healthcare) were used to prepare a calibration curve. The elution volumes (V_e) of standard proteins (ferritin, catalase, aldolase, coalbumin, ovalbumin, ribonuclease A) were used to calculate their corresponding partition coefficient, K_{AV}—eqn (1). Blue dextran 2000 (GE Healthcare) was used to determine the void volume (V_0). V_t is the total bead volume of the column. The K_{AV} value for each protein was plotted against the log of their corresponding molecular mass, yielding a linear function with the values for the y-intercept and the slope given in eqn (2). A final volume of 100 μL of recombinant enzyme sample was applied to the column at three distinct concentrations (7 μM, 11 μM and 53 μM) to determine the V_e value for *Mt*OPRT. Substitution of the latter in eqn (2) allowed determination of the molecular mass of recombinant enzyme in its apo form in solution.

$$K_{AV} = \frac{V_e - V_0}{V_t - V_0} \quad (1)$$

$$K_{AV} = 0.9669 - 0.3087 \log \text{kDa} \quad (2)$$

Enzymatic activity assay

All chemicals in enzyme activity measurements were purchased from Sigma Aldrich. *Mt*OPRT activity was measured both for the forward (phosphoribosyltransferase) and reverse (pyrophosphorolysis) reactions, by a continuous assay measuring, respectively, a decrease or increase in OA concentration. The assay was performed in quartz cuvettes with a UV-visible Shimadzu spectrophotometer UV2550 equipped with a temperature-controlled cuvette holder. For the forward reaction (OA + PRPP → OMP + PP_i), the reaction mixture (500 μL)

contained Tris HCl 50 mM, $MgCl_2$ 20 mM, pH 8.0 and varied concentrations of OA and PRPP. Reaction was started by addition of enzyme, and followed a linear progress of absorbance change at 295 nm for 60 s at 25 °C. The extinction coefficient of this conversion was 3950 M^{-1} cm^{-1}.[33] For the reverse reaction (OMP + PP_i → OA + PRPP), the reaction mixture (500 μL) contained Tris HCl 50 mM, $MgCl_2$ 20 mM, pH 8.0 and varied concentrations of OMP and PP_i. Reaction was started by addition of enzyme, and followed a linear progress of absorbance change at 303 nm for 60 s at 25 °C. The extinction coefficient of this conversion was 2200 M^{-1} cm^{-1}.[43]

Steady-state kinetics

Kinetic assays for forward and reverse reactions were performed using homogeneous *Mt*OPRT (25–50 nM per reaction), under the same assay conditions as described above. For optimal $MgCl_2$ concentration determination, saturating concentrations of OA (100 μM) and PRPP (500 μM) were employed and *Mt*OPRT concentration was 98 nM. $MgCl_2$ concentration was varied from 0 to 30 mM, in Tris HCl 50 mM, pH 8.0, at 25 °C. The decrease in OA concentration was monitored at 295 nm. Based on these results, subsequent experiments employed $MgCl_2$ at fixed 20 mM concentration (Tris HCl 50 mM, $MgCl_2$ 20 mM, pH 8.0—buffer D). K_M and V_{max} values for OA, PRPP, OMP and PP_i were determined by initial velocity measurement in duplicate or triplicate with at least five substrate concentrations. In the forward reaction, a 500 μL final volume reaction contained buffer D and 2–100 μM OA and 25–500 μM PRPP. In the reverse reaction, K_M^{app} and V_{max}^{app} were determined in a 500 μL final volume reaction containing buffer D and varied OMP concentrations (2–12 μM) in the presence of PP_i 100 μM and varied PP_i concentrations (6–105 μM) in the presence of 400 μM OMP. The k_{cat} values were calculated from eqn (3).[53]

$$V_{max} = k_{cat}[E]_t \quad (3)$$

Data from initial velocity double reciprocal plots for the forward reaction were initially fitted to eqn (4) for double-displacement or Ping-Pong bisubstrate kinetic mechanism using SigmaPlot 10 Software; in which v, V, A, and B correspond to, respectively, steady-state reaction rate, maximum reaction rate (V_{max}), substrate A and substrate B concentrations. K_a and K_b are the K_M values for substrate A and substrate B.

$$v = \frac{VAB}{K_aB + K_bA + AB} \quad (4)$$

PP_i detection assay

Release of PP_i by *Mt*OPRT in the forward reaction was monitored indirectly using an EnzCheck® Pyrophosphate Assay E-6645 detection kit (Molecular Probes, Invitrogen). This kit employs two enzymes in a coupled assay to measure changes in PP_i concentration. First, PP_i released by *Mt*OPRT reaction is converted to P_i by inorganic pyrophosphatase. Second, the P_i released into solution is a co-substrate for phosphorolysis of 2-amino-6-mercapto-7-methylpurine ribonucleoside (MESG) into ribose 1-phosphate and 2-amino-6-mercapto-7-methylpurine catalyzed by purine nucleoside phosphorylase (PNP). Enzymatic conversion of MESG into 2-amino-6-mercapto-7-methylpurine was measured at 360 nm ($\Delta\varepsilon_{360nm}$ 11 000 $M^{-1}cm^{-1}$) which is the result of a spectrophotometric shift in maximum absorbance from 330 nm for the substrate to 360 nm for the product. The PP_i detection assay was performed at 22 °C, in a final 500 μL reaction volume containing buffer D, MESG 1 mM, PNP 100 U mL^{-1}, inorganic pyrophosphatase 3 U mL^{-1}, PRPP 5–40 μM and *Mt*OPRT 50 nM, in either the presence or absence of OA 100 μM. PRPP was varied in a range where PNP catalyzed P_i consumption was linear under the assay conditions. All reagents were incubated for 10 min at 22 °C and the reaction was started by addition of *Mt*OPRT.

Product inhibition assays

Product inhibition assays were carried out in 500 μL reaction volume at 25 °C, monitoring the decrease in OA concentration upon conversion to OMP at 295 nm for 60 s. These assays employed either a constant saturating concentration (5 times its K_M value) or sub-saturating concentration (half its K_M value) of one substrate, and varying concentrations of the co-substrate (OA: 6–75 μM, PRPP: 25–400 μM), in the absence and presence of varying concentrations of each product (OMP: 3–60 μM, PP_i: 25–125 μM). Product inhibition assays were performed in buffer D, and the enzyme-catalyzed chemical reactions started upon addition of 25–50 nM *Mt*OPRT to assay mixtures. Double reciprocal data were fitted to eqn (5) for a noncompetitive inhibition mechanism, in which v, V, A, K, K_i, and α correspond to, respectively, steady-state reaction rate, maximum reaction rate (V_{max}), varying concentrations of substrate A, Michaelis–Menten constant, inhibition dissociation constant, and the factor α reflects the effect of inhibitor on the affinity of the enzyme for its substrate (or the effect of the substrate on the affinity of the enzyme for the inhibitor).

$$v = \frac{VA}{A\left(1 + \frac{I}{\alpha K_i}\right) + K\left(1 + \frac{I}{K_i}\right)} \quad (5)$$

ITC binding assays

Ligand binding to *Mt*OPRT was evaluated by isothermal titration calorimetry (ITC) using an iTC_{200} Microcalorimeter (Microcal, Inc., Northampton, MA). Reference cell (200 μL) was loaded with Millie-Q water during all assays. The injection syringe (39.7 μL) was filled with substrate(s) or product(s) at different concentrations (PRPP 4 mM, OA 9 mM, OMP 750 μM and PP_i 10 mM), and the ligand binding isotherms were measured by direct titration (ligand into macromolecule). First injection (0.5 μL) of ligand was followed by seventeen injections of 2.26 μL each spaced by 180 s, into 100 μM apo *Mt*OPRT (sample cell). The titration value of first injection was not used in data analysis. *Mt*OPRT and all ligand solutions contained $MgCl_2$ 20 mM in buffer Gly-Gly 100 mM, pH 8.0 (buffer E), the latter substituted for buffer D due to the high enthalpy of ionization of Tris.[71] Control titrations (ligand into buffer) were performed to subtract the heats of dilution and mixing for each experiment prior to data analysis. To assess *Mt*OPRT:PP_i:OA dead-end complex formation, *Mt*OPRT (90 μM) was incubated with PP_i (900 μM) in the

sample cell prior to OA titration (800 μM syringe concentration). *Mt*OPRT:PP_i:OA ternary complex formation was also assessed by pre-incubating *Mt*OPRT (90 μM) with OA (800 μM), followed by titration with PP_i (900 μM syringe concentration). ITC data were fitted to eqn (6), in which ΔH is the enthalpy of binding, ΔG is the Gibbs free energy change, ΔS is the entropy change, T is the absolute temperature in Kelvin, R is the gas constant (1.987 cal K^{-1} mol^{-1}), and K_a is the association constant. The dissociation constant, K_d, was calculated as the inverse of K_a. All data were evaluated using the Origin 7 SR4 software (Microcal, Inc.). Entropy values are depicted as $-T\Delta S$.

$$\Delta G = \Delta H - T\Delta S = -RT \ln K_a \quad (6)$$

Re-examination of steady-state kinetic data

The steady-state kinetics data were re-examined in light of conflicting results from half-reaction measurements, product inhibition data, and ITC assays. Accordingly, data from initial velocity double reciprocal plots for the forward reaction were fitted to eqn (7) for an Ordered Bi–Bi system using SigmaPlot 10 Software. For eqn (7), K_{ia} represents the equilibrium dissociation constant of substrate A from the binary complex; whereas definitions of v, V, K_a, K_b, A, and B are the same as for eqn (4).

$$v = \frac{VAB}{K_{ia}K_b + K_aB + K_bA + AB} \quad (7)$$

Acknowledgements

This work was supported by funds of Decit/SCTIE/MS-MCT-CNPq-FNDCT-CAPES to National Institute of Science and Technology on Tuberculosis (INCT-TB) to D.S.S. and L.A.B. L.A.B. and D.S.S. also acknowledge financial support awarded by FAPERGS-CNPq-PRONEX-2009. D.S.S. (CNPq, 304051/1975-06) and L.A.B. (CNPq, 520182/99-5) are Research Career Awardees of the National Research Council of Brazil (CNPq). A.B., L.A.R. and D.M.L. acknowledge scholarships awarded by, respectively, BNDES, CAPES and PNPD-CAPES.

References

1 R. G. Ducati, *et al*., *Mem. Inst. Oswaldo Cruz*, 2006, **101**, 697–714.
2 World Health Organization. *Global Tuberculosis Control - Epidemiology, Strategy, Financing*. (August, 2009). www.who.int/tb/publications/global_report/2009.
3 World Health Organization, *Global tuberculosis control: a short update to the 2009 report*, WHO Press, Switzerland, 2010.
4 A. A. Velayati, M. R. Masjedi, P. Farnia, P. Tabarsi, J. Ghanavi, A. H. ZiaZarifi and S. E. A. A. Hoffner, *Chest*, 2009, **136**, 420–425.
5 A. A. Velayati, P. Farnia, M. R. Masjedi, T. A. Ibrahim, P. Tabarsi, R. Z. Haroun, H. O. Kuan, J. Ghanavi, P. Farnia and M. Varahram, *Eur. Respir. J*., 2009, **34**, 1202–1203.
6 J. E. Gomez and J. D. MdKinney, *Tuberculosis*, 2004, **84**, 29–44.
7 T. R. Rustad, A. M. Sherrid, K. J. Minch and D. R. Sherman, *Cell. Microbiol*., 2009, **11**, 1151–1159.
8 W. Eisenreich, T. Dandekar, J. Heesemann and W. Goebel, *Nat. Rev. Microbiol*., 2010, **8**, 401–412.
9 M. Niederweis, *Microbiology*, 2008, **154**, 679–692.
10 B. Raupach and S. H. E. Kaufmann, *Curr. Opin. Immunol*., 2001, **13**, 417–428.
11 J. M. Davis and L. Ramakrishnan, *Cell (Cambridge, Mass.)*, 2009, **136**, 38–49.
12 R. G. Ducati, A. Breda, L. A. Basso and D. S. Santos, *Curr. Med. Chem*., 2010, **18**, 1258–1275.
13 B. A. Fox and D. J. Bzik, *Nature*, 2002, **415**, 926–930.
14 S. R. Krungkrai, S. Aoki, N. M. Q. Palacpac, D. Sato, T. Mitamura, J. Krungkrai and T. Horii, *Mol. Biochem. Parasitol*., 2004, **134**, 245–255.
15 T. D. Bold and J. D. Ernst, *Cell (Cambridge, Mass.)*, 2009, **136**, 17–19.
16 L. S. Meena and Rajni, *FEBS J*., 2010, **277**, 2416–2427.
17 A. D. Tischler and J. D. McKinney, *Curr. Opin. Microbiol*., 2010, **13**, 93–99.
18 H. I. M. Boshoff and C. E. Barry 3rd, *Nat. Rev. Microbiol*., 2005, **3**, 70–80.
19 D. G. Russel, *Nat. Rev. Microbiol*., 2007, **5**, 39–47.
20 G. A. O'Donovan and J. Neuhard, *Bacteriol. Rev*., 1970, **34**, 278–343.
21 C. M. Sassetti, H. B. Dana and E. J. Rubin, *Mol. Microbiol*., 2003, **48**, 77–84.
22 S. T. Cole, *et al*., *Nature*, 1998, **393**, 537–544.
23 R. W. McClard, E. A. Holets, A. L. MacKinnon and J. F. Witte, *Biochemistry*, 2006, **45**, 5330–5342.
24 M. B. Bhatia, A. Vinitsky and C. Grubmeyer, *Biochemistry*, 1990, **29**, 10480–10487.
25 G. P. Wang, C. Lundegaard, K. F. Jensen and C. Grubmeyer, *Biochemistry*, 1999, **38**, 275–283.
26 X. Wang, C. Ma, X. Wang and P. Xu, *J. Bacteriol*., 2007, **189**, 9030–9036.
27 M. J. Yablonski, D. A. Pasek, B. D. Han, M. E. Jones and T. W. Traut, *J. Biol. Chem*., 1996, **271**, 10704–10708.
28 K. L. Rebholz and D. B. Northrop, *Methods Enzymol*., 1995, **249**, 211–240.
29 R. A. Copeland, *Evaluation of Enzyme Inhibitors in Drug Discovery*, John Wiley & Sons, 1st edn, 2005.
30 A. Henriksen, N. Aghajari, K. F. Jensen and M. Gajhede, *Biochemistry*, 1996, **35**, 3803–3809.
31 G. Dodin, *FEBS Lett*., 1981, **134**, 20–24.
32 D. O. Bayles, G. J. Fennington Jr. and T. A. Hughes, *Gene*, 1997, **195**, 329–336.
33 S. R. Krungkrai, B. J. DelFraino, J. A. Smiley, P. Prapunwattana, T. Mitamura, T. Horii and J. Krungkrai, *Biochemistry*, 2005, **44**, 1643–1652.
34 K. Umezu, *et al*., *J. Biochem*., 1971, **70**, 249–262.
35 J. Victor, A. Leo-Mensah and D. L. Sloan, *Biochemistry*, 1979, **18**, 3597–3604.
36 M. B. Bhatia and C. Grubmeyer, *Arch. Biochem. Biophys*., 1993, **302**, 321–325.
37 P. Poulsen, K. F. Jensen, P. Valentin-Hansen, P. Carlsson and L. G. Lundberg, *Eur. J. Biochem*., 1983, **135**, 223–229.
38 G. P. Wang, S. M. Cahill, X. Liu, M. E. Girvin and C. Grubmeyer, *Biochemistry*, 1999, **38**, 284–295.
39 S. C. Sinha and J. L. Smith, *Curr. Opin. Struct. Biol*., 2001, **11**, 733–739.
40 M. A. Schumacher, D. Carter, D. S. Roos, B. Ullman and R. G. Brennan, *Nat. Struct. Biol*., 1996, **3**, 881–887.
41 J. L. Smith, *Nat. Struct. Biol*., 1999, **6**, 502–504.
42 L. González-Segura, J. F. Witte, R. W. McClard and T. D. Hurley, *Biochemistry*, 2007, **46**, 14075–14086.
43 D. H. Ozturk, R. H. Dorfman, G. Scapin, J. C. Sacchettini and C. Grubmeyer, *Biochemistry*, 1995, **34**, 10755–10763.
44 C. Grubmeyer, E. Segura and R. Dorfman, *J. Biol. Chem*., 1993, **268**, 20299–20304.
45 H. Hamana and T. Shinozawa, *J. Biochem*., 1999, **125**, 109–114.
46 S. R. Kungkrai, P. Prapunwattana, T. Horii and J. Krungkrai, *Biochem. Biophys. Res. Commun*., 2004, **318**, 1012–1018.
47 P. Kanchanaphum and J. Kungkrai, *Biochem. Biophys. Res. Commun*., 2009, **309**, 337–341.
48 G. Scapin, D. H. Ozturk, C. Grubmeyer and J. C. Sacchettini, *Biochemsitry*, 1995, **34**, 10744–10754.
49 D. H. Ozturk, R. H. Dorfman, G. Scapin, J. C. Sacchettini and C. Grubmeyer, *Biochemistry*, 1995, **34**, 10764–10770.
50 G. Scapin, C. Grubmeyer and J. C. Sacchetinni, *Biochemistry*, 1994, **33**, 1287–1294.
51 C. P. Liu, *et al*., *Acta Crystallogr., Sect. F: Struct. Biol. Cryst. Commun*., 2010, **66**, 498–502.

52 J. F. Witte, R. Tsou and R. W. McClard, *Arch. Biochem. Biophys.*, 1999, **361**, 106–112.
53 I. H. Segel, *Enzyme kinetics—Behavior analysis of rapid equilibrium and steady-state enzyme systems*, Wyley-Interscience Publication, John Wiley & Sons, Inc., 1993.
54 J. Bar-Tana and W. W. Cleland, *J. Biol. Chem.*, 1974, **249**, 1271–1276.
55 B. F. Cooper and F. B. Rudolph, *Methods Enzymol.*, 1995, **249**, 188–210.
56 D. B. Northrop and K. L. Rebholz, *Arch. Biochem. Biophys.*, 1997, **342**, 317–321.
57 V. Leskovac, *Comprehensive enzyme kinetics*, Kluwer Academic, Plenum Publishers, New York, 2003.
58 R. O'Brien and I. Haq, *Applications of Biocalorimetry: Binding, Stability and Enzyme Kinetics*, *Biocalorimetry 2 Applications of calorimetry in the biological sciences*, ed. J. E Ladbury, M. L Doyle, John Wiley & Sons, 2004, pp. 3–34.
59 M. R. Eftink, A. C. Anusiem and R. L. Biltonen, *Biochemistry*, 1983, **22**, 3884–3896.
60 A. Brown, *Int. J. Mol. Sci.*, 2009, **10**, 3457–3477.
61 R. Zaleskis, *Eur. Respir. Dis.*, 2006, 47–49.
62 Z. Ma, C. Lienhardt, H. MdIlleton, A. J. Nunn and X. Wang, *Lancet*, 2010, **375**, 2100–2109.
63 N. N. Umejiego, C. Li, T. Riera, L. Hedstrom and B. Striepen, *J. Biol. Chem.*, 2004, **279**, 40320–40327.
64 A. Dhar, A. Samiotakis, S. Ebbinghaus, L. Nienhaus, D. Homouz, M. Gruebele and M. S. Cheung, *Proc. Natl. Acad. Sci. U. S. A.*, 2010, **107**, 17586–17591.
65 M. M. Bradford, *Anal. Biochem.*, 1976, **72**, 248–254.
66 H. Edelhoch, *Biochemistry*, 1967, **6**, 1948–1954.
67 C. N. Pace, F. Vajdos, L. Fee, G. Grimsley and T. Gray, *Protein Sci.*, 1995, **4**, 2411–2423.
68 U. K. Laemmli, *Nature*, 1970, **227**, 680–685.
69 A. Shevchenko, M. Wilm, O. Vorm and M. Mann, *Anal. Chem.*, 1996, **68**, 850–858.
70 Z. Zhang and A. G. Marshall, *J. Am. Soc. Mass Spectrom.*, 1998, **9**, 225–233.
71 H. Fukada and K. Takahashi, *Proteins: Struct., Funct., Genet.*, 1998, **33**, 159–166.
72 J. D. Thompson, D. G. Higgins and T. J. Gibson, *Nucleic Acids Res.*, 1994, **22**, 4673–4680.

